**Proceedings of ASME Turbo Expo 2011**
**GT2011**
**June 6-10, 2011, Vancouver, British Columbia, Canada**

# GT2011-45296

# EXPERIMENTAL INVESTIGATIONS ON COOLING AIR EJECTION AT A STRAIGHT TURBINE CASCADE USING PIV AND QLS

**Oliver Freund**
Institute of Turbomachinery and Fluid Dynamics
Leibniz Universität Hannover
Appelstraße 9
DE-30167 Hannover, Germany
Email: freund@tfd.uni-hannover.de

**Hans-Juergen Rehder**
German Aerospace Center
Turbine Group
Bunsenstraße 10
DE-37073 Göttingen, Germany
Email: hans-juergen.rehder@dlr.de

**Philipp Schaefer**
German Aerospace Center
Turbine Group
Bunsenstraße 10
DE-37073 Göttingen, Germany
Email: philipp.schaefer@dlr.de

**Ingo Roehle**
German Aerospace Center
Leader of the Turbine Group
Bunsenstraße 10
DE-37073 Göttingen, Germany
Email: ingo.roehle@dlr.de

## ABSTRACT

*Due to the high turbine inlet temperatures in modern aircraft engines the adoption of several cooling techniques in the first turbine blade rows is state of the art. For this reason the influence of cooling air ejection on the main flow is in the interest of scientists. In this paper experimental and numerical investigations on the trailing edge cooling air ejection at a stator profile are presented. All measurements are performed at the Straight Cascade Wind tunnel Göttingen. To verify the influence of the cooling air flow on the flow field, the velocity field is measured by Particle Image Velocimetry (PIV). The development of the cooling air concentration is analyzed by utilizing the Quantitative Light Sheet (QLS) technique. For validation purposes the QLS results are compared to $CO_2$ concentration measurements. Both measurement techniques are in good agreement with each other. One of the most important advantages of PIV and QLS is the possibility of combining them at the same test bed due to the identical experimental setup. The experimental investigations are supported by numerical simulations based on the numerical code TRACE. Both the numerical results as well as the experimental results prove the reduction of the trailing edge shock by increasing the coolant mass flow ratio.*

## NOMENCLATURE

| latin symbols | | indices | |
|---|---|---|---|
| $C$ | rel. concentration | $0$ | total |
| $c_m$ | coolant mass flow ratio | $1$ | inlet |
| $D$ | dark current | $2$ | outlet |
| $F$ | illustration factor | $C$ | cooling air |
| $H$ | background | $g$ | global |
| $I$ | detected light intensity | $is$ | isentropic |
| $I_L$ | light sheet intensity | $max$ | maximum |
| $K$ | angle coefficient | $ps$ | pressure side |
| $\dot{m}$ | mass flow | $sb$ | single blade |
| $Ma$ | Mach number | $ss$ | suction side |
| $P$ | number of particles | | |
| $R$ | gas constant of air | | |
| $T$ | temperature | | |
| $U$ | Velocity | | |

**greek symbols**

| | |
|---|---|
| $\Delta s$ | displacement |
| $\Delta t$ | time delay |
| $\kappa$ | isentropic coefficient |
| $\sigma$ | standard deviation |

## INTRODUCTION

One of the main efforts in development of turbomachinery is the reduction of the specific fuel consumption. By increasing the turbine inlet temperature, coupled with higher compressor pressure ratios, the overall efficiency of turbomaschines can be improved (Wilcock et al [1]). Nowadays turbine inlet temperatures already exceeded the melting point of the material used for the first blade rows. For this purpose different cooling methods are needed to prevent the turbine blades from failure (Bunker [2]). In addition to internal cooling methods, e.g. convective and impingement cooling, external methods like film cooling and trailing edge cooling air ejection are implemented. Especially the inlet guide vanes (IGV) need an effective cooling. Due to aerodynamic aspects the trailing edge has to be as thin as possible. Therefore, this part of the blade is particular vulnerable (Martini et al. [3]). Beside the benefit of higher realizable inlet turbine temperatures by cooling the trailing edge there are negative effects on the main turbine parameters. These effects are caused by the unavoidable thickening of the trailing edge and the interference of the cooling air flow with the main flow. A common way to reduce the trailing edge thickness is the cut back of the material on the pressure side (Chen et al. [4]).

In the past different studies concerning the trailing edge cooling air ejection has been performed. Sieverding [5] presents a detailed investigation of a single blade configuration with a slot at the trailing edge. The essentially thickened trailing edge of the investigated blade geometry enables detailed pressure measurements close to the slot. An empirical function for the back pressure is evaluated from these tests. Kapteijn et al. [6] investigate an internally cooled turbine guide vane. The study includes a comparison of two basically identical blade geometries except the varied coolant flow exit. In addition to determined Mach number distributions at the blade surfaces coolant air concentration measurements are carried out by a $CO_2$ concentration measurement technique. Kost and Raffel [7] investigate the aerodynamic effects of trailing edge cooling air ejection at a turbine blade model. Concerning the losses this study indicates the existence of an optimum coolant mass flow ratio.

In the past the measurement of the flow velocity and the cooling air concentration are mainly performed using probe measurement methods. Using modern optical techniques, e.g. PIV, allows the planar measurement of the flow parameters, which leads to a considerable benefit concerning the testing time.

Therefore, this paper deals with an investigation on a stator profile with internal cooling using the well known PIV and the QLS measurement technique. The QLS technique is a concentration measurement method based on the scattered light of seeding particles and was published by Voigt and Schodl [8], Voigt [9], and Hassa et al. [10]. The QLS technique is often used for analyzing mixing processes in combustion chambers (Jakirlić et al. [11], Gnirß and Tropea [12]). Additionally, it is also a suitable method for analyzing the cooling air ejection of turbine blades as primarily shown by Langwosky [13], who investigated film cooled turbine blades using the QLS technique. To go one step further, this paper points at additional validation of the QLS technique concerning measurements on cooling air ejection of turbine blades. All experiments of the present paper are carried out in an ambient flow suction type cascade wind tunnel (EGG) at DLR Göttingen.

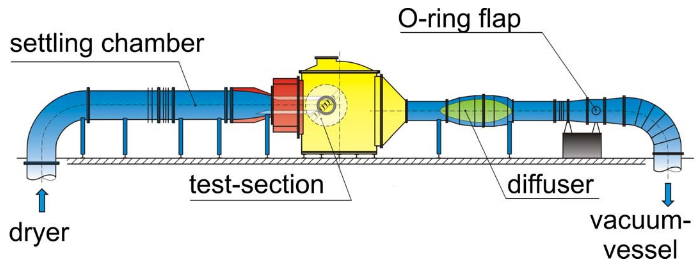


**FIGURE 1**. Straight Cascade Wind tunnel EGG at DLR Göttingen

## EXPERIMENTAL AND NUMERICAL INVESTIGATIONS

### Test rig

In general the flows in turbomachinery are unsteady, three-dimensional, and highly turbulent. To reduce the flow in its complexity, the usage of a straight cascade model is very helpful for experimental investigations. Two simplifications of the straight cascade flow in contrast to real three-dimensional turbomachinery flows make it possible to investigate a nearly two-dimensional flow. First, the cascade profile is based on an infinitely long linear development of a coaxial cylindrical intersection of the investigated turbomachine blade row. Secondly, there are no Coriolis or centrifugal forces acting on the flow due to the fact that the blades are fixed.

The setup of the EGG Göttingen is shown in Fig. 1. As already mentioned it is an ambient flow suction wind tunnel. Ambient air is sucked from the atmosphere through the test section into a vacuum vessel. The vacuum vessel whose volume is about 10000 $m^3$ is evacuated by two 250 kW water ring pumps. Before the air enters the test section its humidity is reduced by a dryer. Afterwards the flow is homogenized in the settling chamber. The wind tunnel can be started and stopped by opening and closing an O-ring flap. By changing the cross-section of the flow at the variable diffuser, which is located downstream of the test section,

 

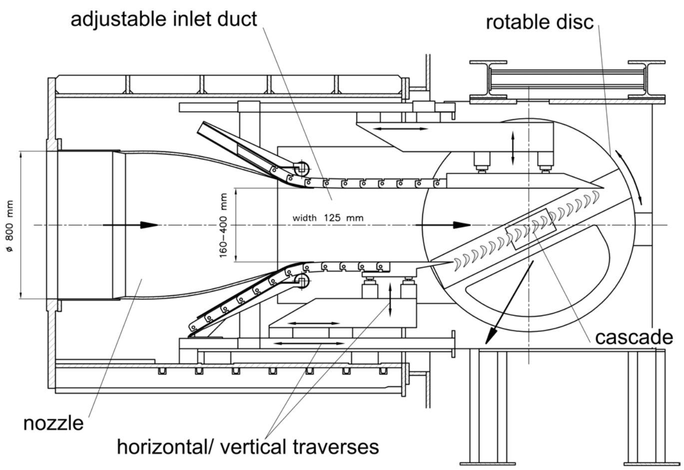


**FIGURE 2**. Test section of the EGG

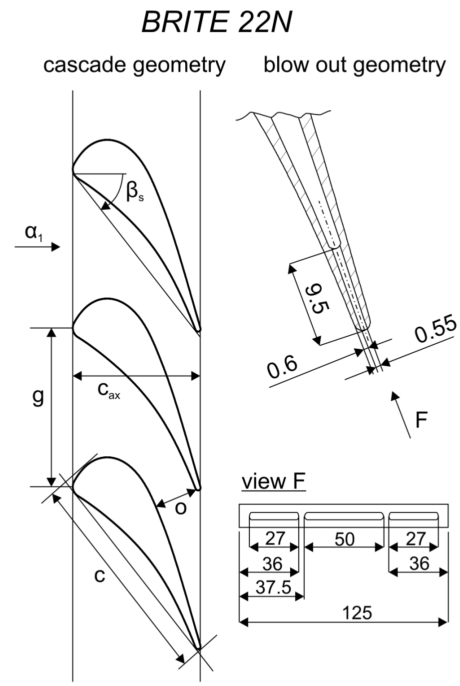


**FIGURE 3**. Cascade geometry (all dimensions in mm)

the flow velocity can be controlled. A closer look at the test section is shown in Fig. 2. The acceleration of the flow is realized by a variable inlet nozzle. Furthermore, the cascade is fixed between two rotatable turntables. The cascade angle of attack can be adjusted by rotating the turntables. The main parameter to characterize the flow of the EGG at DLR is the isentropic outlet Mach number which is defined by:

$$Ma_{2,is} = \sqrt{\frac{2}{\kappa - 1}\left[\left(\frac{p_{01}}{p_2}\right)^{\frac{\kappa-1}{\kappa}} - 1\right]} \tag{1}$$

The total pressure $p_{01}$ is measured in the settling chamber at a very low velocity of the flow, the static pressure $p_2$ (back pressure of the cascade) is measured in the test chamber. The realizable range of isentropic Mach numbers at the EGG Göttingen is between 0.2 and 1.6.

The investigated stator profile BRITE22N is shown in Fig. 3. The profile is internally cooled. The cooling air is blown out through a slot at the trailing edge. A detailed description of investigations, which were performed on this profile, is given by Dunker [14]. The main cascade parameters are shown in Tab. 1. The chord length of 72 mm results in a Reynolds number for $Ma_{2,is}$=0.2..1.05 from $0.34 \cdot 10^6$ to $1.01 \cdot 10^6$.

Figure 4 illustrates the seeding setup and the cooling air supply. The main flow is seeded at two positions to achieve a homogeneous particle distribution. The cooling air mass flow can be controlled by the valve of the cooling air supply line. After the cooling air mass flow is seeded it is measured by an orifice and distributed to the different blades of the cascade.

## Measurement techniques

In order to determine the influence of the cooling air ejection on the main flow two optical measurement techniques are used. As already mentioned one advantage of the PIV and the QLS technique is the same experimental setup. For both measurement techniques the flow has to be seeded. In this paper di-ethyl-hexyl-sebacat (DEHS) is used for generating seeding particles. The distribution of the seeding particles diameter is Gaussian with a mean diameter of 1 $\mu$m. Two Nd:YAG pulse lasers illuminate the measurement plane. The wavelength of the emitted light is 532 nm. A CCD camera captures images of the illuminated plane. The velocity field in the cascade passage, especially in the region of the trailing edge, is measured by PIV. 200 double images are taken and processed in four steps. First, the signal to noise ratio of the raw data is increased by subtracting

**TABLE 1**. Cascade parameters

| | BRITE22N | | |
|---|---|---|---|
| stagger angle $\beta_s$ | 51,9° | chord length c [mm] | 72 |
| pitch g [mm] | 54,07 | inlet flow angle $\alpha_1$ | 0° |
| throat o [mm] | 14,97 | ax. chord length $c_{ax}$ [mm] | 43,07 |
| pitch ratio g/c | 0,751 | profile's height h [mm] | 125 |

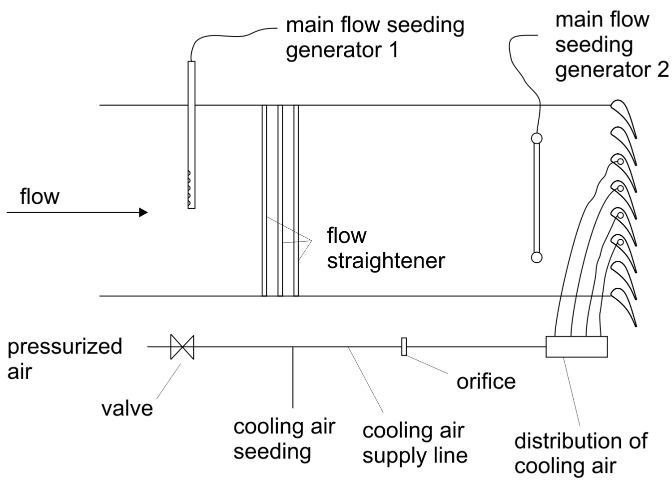


**FIGURE 4**. Seeding setup and cooling air supply

a minimum image. The minimum image consists of the minimal detected light intensity of each pixel of an ensemble of pictures. To take temporary effects like seeding particle deposition at the background into account, the ensemble of pictures for calculating the minimal image is given by a sliding range around the actual processed picture. This method is illustrated by Fig. 5. For example, the minimum image subtracted from the tenth picture is calculated from image 1 to image 31.

The second step is the calculation of the particle displacement to derive the flow velocity. For this purpose the images are divided in equal windows, so called interrogation windows. In the present paper a multigrid method is used. The size of the starting interrogation windows is 96x96 px$^2$ and is reduced in three iteration steps to 32x32 px$^2$. The used overlap of 50% results in a minimal solvable region of 16x16 px$^2$, which represents an area of 0.73x0.73 mm$^2$ based on the illustration factor of the experimental setup. A typical value for the delay between the two pictures is about $\Delta$t=1$\mu s$ for the investigated flow velocities from $Ma_{2,is}$=0.2 to $Ma_{2,is}$=1.05. To prevent the particles from leaving the interrogation window, the maximum displacement of the particles is limited by the adjustment of the time delay in dependency on the investigated flow velocity. For determination of the particle displacement in subpixel range the least squares method is used.

The accuracy of the interpolation scheme (least squares method) used in this paper can be concluded from a numerical study performed by Nobach et al. [15]. In this study the RMS error of different interpolation schemes is investigated by processing four different test cases. The particle mapping value of the PIV measurements presented in this paper is 1 pixel which leads to a RMS error of 0.06 pixel. Under consideration of the time delay between the double images this results in a maximum error of $\Delta Ma_{2,is} = 0.01$.

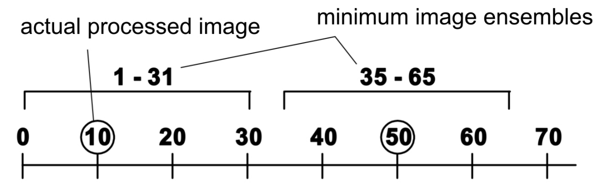


**FIGURE 5**. Generation of minimum image

The next very important step of processing is the validation of the vector field. Four filters are used to detect and eliminate outliers. The first filter is the maximum allowed displacement. It is set to the maximum displacement in the measurement plane additionally multiplied with a assessment factor of two. In the second step of validation the calculated displacement is checked by the normalized median test. This test method determines the central value of a 3x3 field of values around the considered value. If the considered value is greater than the threshold, it is declared as an outlier. The filter threshold is given by the central value multiplied by a factor. In this paper a factor of five is used. In addition, a standardization automatically adjust the filter threshold to the local flow conditions. In this way it is assured that in areas of high fluctuation the normalized median test restriction is lowered. The third filter, the dynamic mean operator, also uses a 3x3 field of values to validate the determined vectors by calculating the mean velocity and its standard deviation. The values $C_1$ and $C_2$ represent two factors to weight the absolute value and the standard deviation in this filter:

$$|U_m - U| < C_1 + C_2 \cdot \sigma \tag{2}$$

The values used in the present paper are $C_1 = 2$ and $C_2 = 1$. The last restriction for validating the vector field is a minimum height of the correlation peak of 30%. A detailed explanation of the used filters is given by Raffel et al. [16].

In the last step the 200 determined vector fields are averaged and the distribution of the local Mach number $Ma_2$ is calculated by

$$Ma_2 = \frac{|U|}{\sqrt{\kappa\, R\, T_0 - \frac{\kappa-1}{2} U^2}} \tag{3}$$

with

$$U = \frac{\Delta s}{F \cdot \Delta t} \tag{4}$$

The flow velocity $U$ is given by the determined displacement $\Delta$s, the time delay between the double image $\Delta$t, and the illustration factor F. For processing the PIV data the software package PIVVIEW 3.0 is used.

Additionally to the measurement of the flow velocity, the development of the cooling air concentration is investigated by the QLS measurement technique. The basic idea of this technique is the unbalance of the inertial particle density, i.e. in the present case the cooling air is seeded in contrast to the main flow. By measuring the light intensity scattered by the illuminated seeding particles a local mixing ratio of the main flow and the cooling air can be determined.

Similar to the PIV measurement technique the QLS raw data has to be divided into several interrogation windows for processing. For each interrogation window the measured intensities of all pixels enclosed in the interrogation window are summed up and divided by the total number of pixels in the interrogation window. Afterwards every single averaged interrogation window intensity is assigned to every pixel of its individual interrogation window. In contrast to other concentration measurement techniques (for example PLIF) the diameter of the seeding particles used in the QLS measurement technique are comparatively large. Due to this fact there are only a small number of seeding particles in one interrogation window. For this reason the effect of marker shot noise is very important for QLS measurements. This effect is based on the fact, that although the local concentration of the investigated flow in a considered interrogation window is constant, the number of seeding particles in this interrogation window can vary over time. This leads to a variance in the detected light depending on the averaged number of seeding particles in one interrogation window: The smaller the average number of particles in an interrogation window is, the stronger is the effect of marker shot noise on the variance of the measured concentration. On the one hand the variance of the QLS measurements increases with smaller interrogation windows, on the other hand the spatial resolution of the concentration measurement is increased by reducing the dimension of the interrogation windows. In the course of a parameter study the optimum interrogation window size for the present setup was determined to 16x16 px$^2$ with 50% overlap, due to the maximum achievable spatial resolution in consideration of an acceptable standard deviation. Comparable parameters are used for spatial averaging of QLS measurements by Gnirß and Tropea [17].

The measurement of the light intensity scattered by the particles is the base of the QLS technique to determine the local mixing ratio. This intensity is superimposed by several systematic errors, which have to be corrected. The following equation describes a simplified model of the detected light intensity presented by Findeisen et al. [18]:

$$I(x,y) = P(x,y)\, I_L(x,y)\, K(x,y) + H(x,y)\, I_{L_g} + D(x,y) \qquad (5)$$

In this model the captured intensity of light consists of three parts. The first part represents the light intensity scattered by the seeding particles and depends on the number of particles $P(x,y)$,

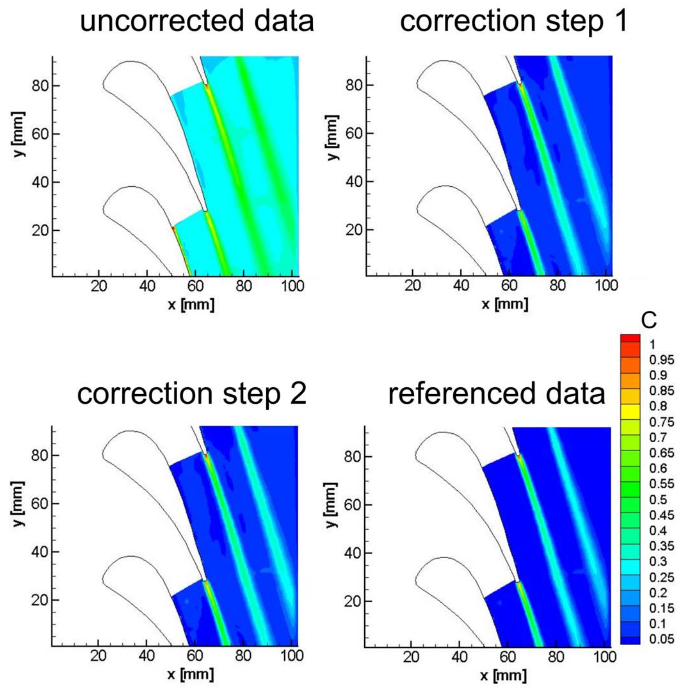


**FIGURE 6**. QLS correction procedure

on the local light sheet intensity $I_L(x,y)$, and on a factor $K(x,y)$ resulting from the different scattering and viewing angles in the measurement plane. Due to the particles diameter, which is in the range of the wavelength of the illuminating laser light, the elastic scattering of light by the particles has to be described by the Mie theory. This is why the influence of the scattering and the viewing angle is significant and has to be taken into account. The second part refers to reflection of light caused by the background. This term consists of the background $H(x,y)$ weighted with the global light sheet intensity $I_{L_g}$. The dark current of the camera represents the third term $D(x,y)$. In reality there are more physical effects influencing the detected light like extinction, passive multi-scattering, and active multi-scattering deduced by Voigt [9]. But these effects can only be taken into account with great efforts under laboratory conditions and are neglected.

To isolate the information of the light intensity scattered by the particles, the raw data has to be processed in different correction steps. The whole correction procedure performed during the QLS measurements in this paper is shown by Fig 6. First, the influence of the reflecting background and the dark current of the camera is minimized. To reduce the reflections the background is painted with low-reflection paint before all measurements. Nevertheless, a reference picture averaged over 200 single images without flow is taken before every measurement. Subtracting the reference picture from the raw data minimizes the influence of the dark current and the background reflections (correction step 1). In the second step the influence of the local light sheet intensity and the scattering and the viewing angle is taken into account. For this purpose a second reference picture also averaged over 200 single images is taken before measurement. In this picture the whole cascade flow is seeded at a very low flow velocity ($v \approx 1$ m/s). In this special case it can be assumed that in the whole measurement plane the local number of seeding particles is constant. For this reason the detected light intensity of this reference picture covers on the one hand the influence of the different local light sheet intensity and on the other hand the angle effects. By dividing the altered raw data by the second reference picture the two parameters $I_L(x,y)$ and $K(x,y)$ of the first term in Eqn. (5) are considered and $P(x,y)$ is isolated (correction step 2). In the last step of the correction procedure the measured intensity of light has to be referenced to achieve the concentration distribution. It is assumed that the concentration of the cooling air directly at the slot exit equals 1. By normalizing the measured light intensities by the intensity value measured directly at the profile trailing edge a concentration distribution can be obtained. $C$ represents the relative concentration of the cooling air mass flow to the main mass flow:

$$C = \frac{\dot{m}_C}{\dot{m}} \tag{6}$$

This assumption leads to the drawback that only qualitative results can be achieved by the QLS measurement technique.

## Numerical simulation

The numerical simulations are performed with the numerical code TRACE (Nürnberger et al. [19], Engel et al. [20, 21]), which solves the 3-D Reynolds-averaged Navier-Stokes equations by using a Finite Volume Method. A structured grid is created and subdivided into blocks to enable parallelization. An upwind method is used to obtain the flow solution on a structured grid at second order accuracy in space. A second order accurate solution in time is achieved by an implicit predictor-corrector scheme. Turbulence is taken into account by the usage of the k-$\omega$ two-equation turbulence model (Wilcox [22]), unphysical overproduction of turbulent kinetic energy at the stagnation point is corrected based on the Cauchy-Schwarz inequality (Durbin et al. [23]). Transition is predicted by using a correlation based model suggested by Menter et al. [24].

In order to reduce computational costs, a 3D-slice containing about 100,000 cells is extracted using symmetric boundary conditions. At the inlet boundary total pressure, total temperature, turbulence intensity, and length scale corresponding to the experiments are set. Furthermore, the outlet pressure is set to the isentropic exit Mach numbers. After about 5000 iterations sufficient convergence is observed resulting in a L1 residual of $10^{-7}$ and a maximal residual of $8 \cdot 10^{-7}$.

## Results

The investigations of cooling air ejection at the BRITE22N stator profile are performed by varying two parameters. The first varied parameter is the isentropic outlet Mach number $Ma_{2,is}$. The straight cascade is investigated at a transonic case ($Ma_{2,is} = 0.8$) and a supersonic case ($Ma_{2,is} = 1.05$). The second variable parameter is the coolant mass flow ratio which is defined by:

$$c_m = \frac{\dot{m}_{C,sb}}{\dot{m}} \tag{7}$$

$c_m$ represents the ratio of the cooling air mass flow blown out from one blade to the main flow of a single blade passage. In the present paper it is varied from 0% to 3% in steps of 1%. The cooling air mass flow is measured by an orifice assembled in the cooling air supply line. The accuracy of the coolant mass flow ratio measurement is $\pm 0.1\%$. The design point of the BRITE22N stator profile is at $Ma_{2,is} = 1.05$ and $c_m = 3\%$.

**PIV - Comparison to numerical results** Figure 7 presents the comparison between the PIV results and the numerical TRACE simulation at the isentropic outlet Mach number $Ma_{2,is} = 1.05$. The coolant mass flow ratio is varied from 0% to 3%. In general, there is a good agreement in the main flow structure. The flow is accelerated along the profile suction side. The trailing edge shock, which is caused by the redirection of the supersonic flow at the trailing edge, decelerates the flow and causes a shock boundary layer interaction on the profile suction side of the adjacent profile. In the region of the profile wake the typical dead water zone can be observed. Concerning the PIV results the region directly behind the trailing edge is especially difficult to measure without cooling air ejection. Only a small number of the main flow tracer particles reach the dead water region at the trailing edge, the major part follows the flow downstream. In the case of cooling air blowing, tracer particles are directly inserted at the trailing edge by the seeded cooling air and the information of velocity near to the trailing edge can be measured. The main differences between simulation and experiment are the resolution of the shock velocity gradient and the velocity distribution of the profile wake. The shock position varies over time since it is an unsteady flow phenomenon. Therefore, the PIV results don't show the shock velocity gradient as high as the numerical results do. Due to their inertia the PIV tracer particles can not instantaneously follow the deceleration of the flow caused by the shock, which also causes a lower shock velocity gradient. The discrepancy concerning the wake is founded in the steadiness of the numerical simulations. For accurate results concerning the wake unsteady simulations have to be performed.

There are two main observable influences of the cooling air ejection on the main flow. To explain the physical background of these effects a sketch of the flow with and without cooling

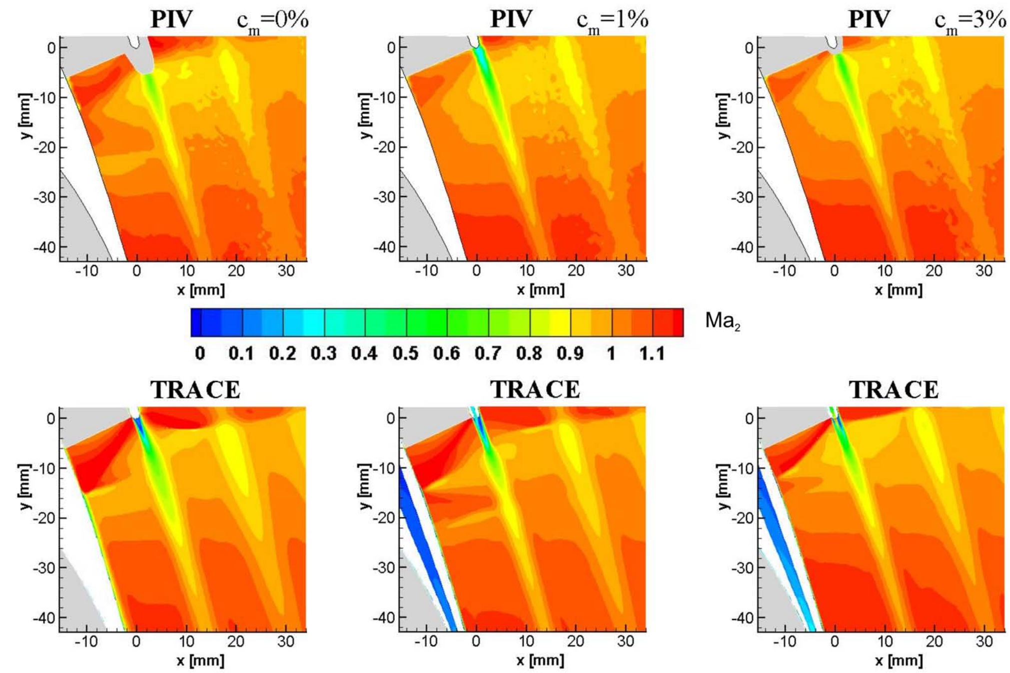


**FIGURE 7**. Comparison between PIV and numerical results

air ejection is presented in Fig. 8. Due to the expanding cross-section the pressure side flow as well as the suction side flow is expanding around the trailing edge if no cooling air is blown out. Further downstream directly at the trailing edge the pressure side flow and the suction side flow unite. This point of union represents a concave edge for the flow, a shock occurs in supersonic flow. This trailing edge shock runs from the point of union to the pressure side of the neighboring profile and causes a shock boundary layer interaction on the profile surface. If the dead water region at the trailing edge is filled by ejecting cooling air, the course of the pressure side flow and the suction side flow changes. The point of the flow redirection and shock origin moves upstream. Furthermore, the flow deflection is reduced, which leads to a decreased intensity of the trailing edge shock.

Both effects can be observed in the numerical and in the experimental results. The comparison of the PIV results at $c_m = 0\%$ and $c_m = 3\%$ shows the movement of the trailing edge shock in upstream direction. Additionally, the attenuation of the trailing edge shock intensity can be observed for increasing $c_m$. The comparison of the numerical results at different coolant mass flow ratios leads to identical conclusions. Furthermore, the numerical simulation at $c_m = 0\%$ calculates a separation of the suction side flow caused by the shock boundary layer interaction of the trailing edge shock. The separation vanishes by increasing $c_m$ due to the decreased intensity of the trailing edge shock. This separation can not be observed in the experimental results, because of the limited spatial resolution of the PIV measurement technique and the negative effect of light reflection at the profile surface. Nevertheless, the existence of a weak shock at the profile pressure side ($x = -9$mm, $y = -20$mm) is an indication for a reattachment point of a separated flow.

Figure 9 shows the standard deviation $Ma_{rms}$ of the PIV measurements. The region between the wake of the upper profile and the suction side of the lower profile is dominated by low standard deviations. $Ma_{rms}$ increases in the region of the wake and the trailing edge shock due to the unsteadiness of these flow phenomena. Furthermore, there is a obvious region of increased $Ma_{rms}$ in the downstream area of the upper profile and the neighboured profile above. The explanation for this effect is the illumination of the flow. The laser light sheet needed for illumination is generated by a cylindrical lens and focused by two spherical lenses. To minimize the reflections of the profile, the light sheet focus is placed parallel to the wake with a certain distance to the profile surface of the lower profile. Because of the thin light sheet at the focus plane there is a higher out-of-plane loss of images which causes an increased $Ma_{rms}$.

The low Mach number PIV results do not provide any additional information concerning the influence of the cooling air ejection which is why they are not discussed in this paper.

### QLS - Comparison to $CO_2$ measurement technique

The concentration distributions of the cooling air at $Ma_{2,is} = 1.05$

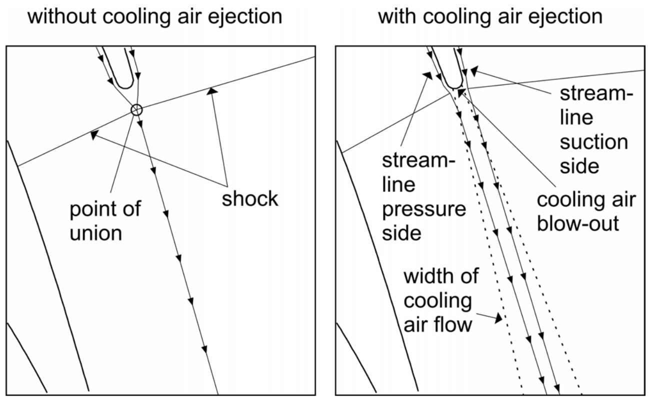


**FIGURE 8**. Shock reducing effect of cooling air blow-out

for different coolant mass flow ratios are shown as contour plots in Fig. 10. The upper plots show an overview of the concentration distribution, in the lower plots the region directly at the trailing edge is zoomed in for detailed analysis. With higher coolant air mass flow ratios an increase of the global cooling air concentration can be observed. The length of the mixing process between the cooling air and the main flow is also extended in flow direction with higher values for $c_m$. Furthermore, there is an obvious deflection of the cooling air to the profile suction side due to the higher pressure on the profile pressure side. The maximum concentration is decreasing with increasing distance to the trailing edge. In addition, the wake width is expanding in flow direction. To analyze the mixing process of the cooling air and the main flow the lower plots of Fig. 10 have to be considered. It becomes clear that the mixing process is caused by the different velocities of the main flow and the coolant flow. For this reason the mixing process begins at the shear layer and continues to the symmetrical axis of the wake. Therefore, the contours of constant cooling air concentration become narrow in flow direction. The cooling air concentration remains longer at higher levels in the wake centre than at the boarder of the wake. Under consideration of the mass conservation and the decrease of maximum cooling air concentration with increasing distance to the trailing edge, the width of the cooling air flow expands.

To analyze the decrease of the maximum concentration of the cooling air and the expansion of the wake width, different concentration curves along vertical lines in different discrete distances to the trailing edge are extracted. For comparison to $CO_2$ concentration measurements performed by Kapteijn summarized in [14] the extracted concentration curves are fitted by Gaussian curves. Because of extracting along vertical lines, instead of extracting perpendicular to the wake axis, the concentration curves are asymmetric. A second cause of asymmetric concentration curves is the difference between the pressure surface and suction surface boundary layer. Due to this asymmetry the concentration curves have to be separated into a pressure side part and a suction side part. For processing reasons the separated curves are mirrored at the point of maximum cooling air concentration. Two Gaussian curves based on the extracted concentrations are calculated:

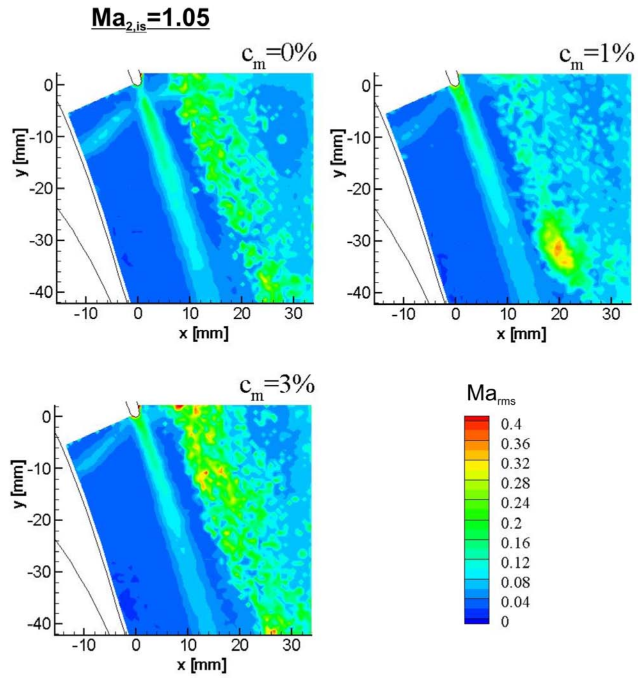


**FIGURE 9**. PIV standard deviation

$$C_{ps} = C_{max} \cdot exp\left(-\frac{(y-\bar{y})}{2\cdot\sigma_{ps}^2}\right) \tag{8}$$

$$C_{ss} = C_{max} \cdot exp\left(-\frac{(y-\bar{y})}{2\cdot\sigma_{ss}^2}\right) \tag{9}$$

To analyze the development of the cooling air concentration, two different parameters are taken into account: the maximum concentration $C_{max}$ and the standard deviations $\sigma_{ss}$ and $\sigma_{ps}$. The standard deviation is an indicator for the width of a Gaussian distribution. For this reason this parameter can be used to identify the development of the cooling air flow width.

The comparison between to the $CO_2$ concentration measurements are shown in Fig. 11 for the transonic case ($Ma_{2,is} = 0.8$) and the supersonic case ($Ma_{2,is} = 1.05$). The maximum concentration and the standard deviation of the Gaussian curves normalized by the pitch are plotted in dependency on the vertical

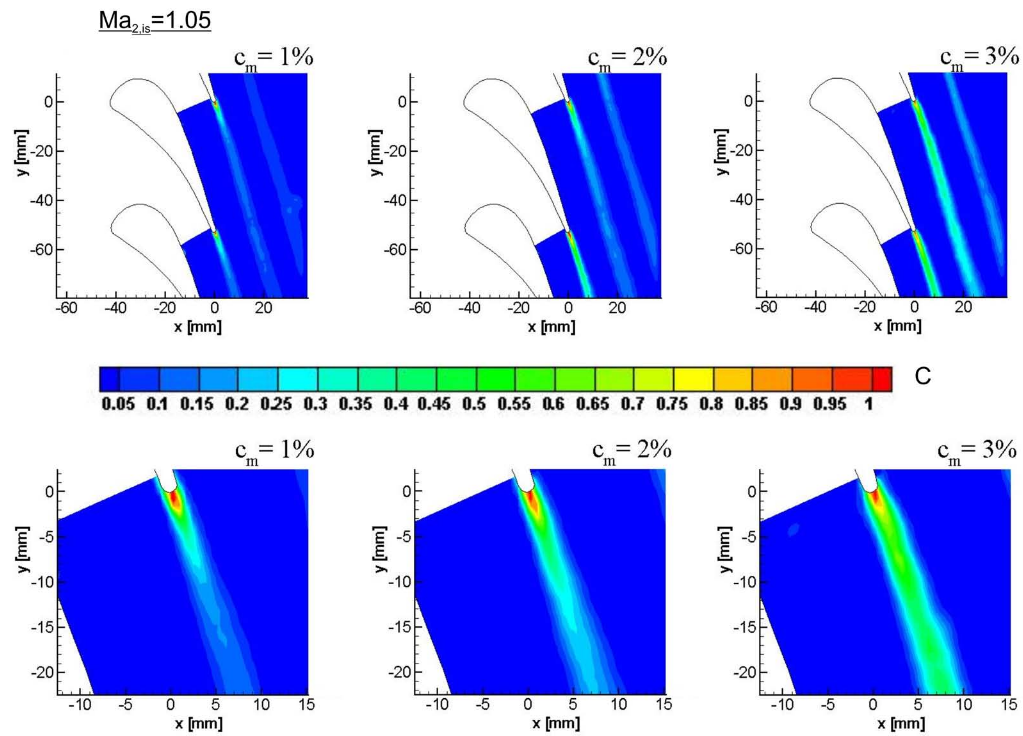


**FIGURE 10**. Concentration distribution

distance to the trailing edge for $c_m = 3\%$. Concerning the curves of maximum cooling air concentration a clear offset between the two measurement techniques can be observed. Because of the referencing step in the procedure of the QLS measurement technique the obtained results are qualitative. For comparison the mean offset between the QLS measurements and the $CO_2$ concentration measurement technique is subtracted.

Due to the author's statement the $CO_2$ measurement technique is used at its limits. Especially for higher Mach numbers there is a high pressure difference between the wake area directly at the blade and the atmosphere. The limitations are caused by the capacity of the vacuum pump and the tradeoff between a small gas sampling probe that disturbs the flow the least and the required gas sampling time to get reliable measurement data. The limits of the $CO_2$ concentration measurements can be concluded in two statements: First, the maximum measureable cooling air concentration is limited. Secondly, there are no reliable concentration data in the wake area directly at the trailing edge for $Ma_{2,is} = 1.05$.

For the transonic case the maximum concentration near to the trailing edge measured by the QLS measurement technique is on a higher level than the $CO_2$ measurements caused by the discussed limits. However, the decrease of the maximum concentration of the QLS measurement technique near to the blade trailing edge is higher than the results of the $CO_2$ measurement technique demonstrate. This difference is due to the different gas types used for cooling air. The higher density of $CO_2$ leads to a lower blowing velocity for an identical coolant mass flow ratio compared to the usage of air for cooling. Therefore, the velocity gradient between the cooling air and the comparable low speed flow at the wake is higher in case of using air for cooling. This leads to an accelerated mixing process. For distances higher than 7 mm to the trailing edge an excellent agreement of the maximum concentration can be observed. The comparison between the standard deviations show the same trend but no agreement in quantitative manner. The increasing values confirm the expansion of the wake by the ongoing mixing process.

In the supersonic flow regime the comparison of the maximum concentration curves is in good agreement as well. The curves of standard deviation shows the same trend again. The slope of the standard deviation shows higher values for this case. This is caused by the higher velocity gradient between the main flow and the cooling air flow. While the main flow velocity is increasing by raising $Ma_{2,is} = 0.8$ to $Ma_{2,is} = 1.05$, the cooling air flow velocity directly at the slot at constant $c_m$ is nearly the same due to the fact, that the main mass flow reaches its limit already at $Ma_{2,is} = 0.9$. A closer look to the standard deviation curves shows a bigger discrepancy between the two measurement techniques at the vertical distance $x = 20$ mm than in the other points. This is caused by the already stated marker shot noise

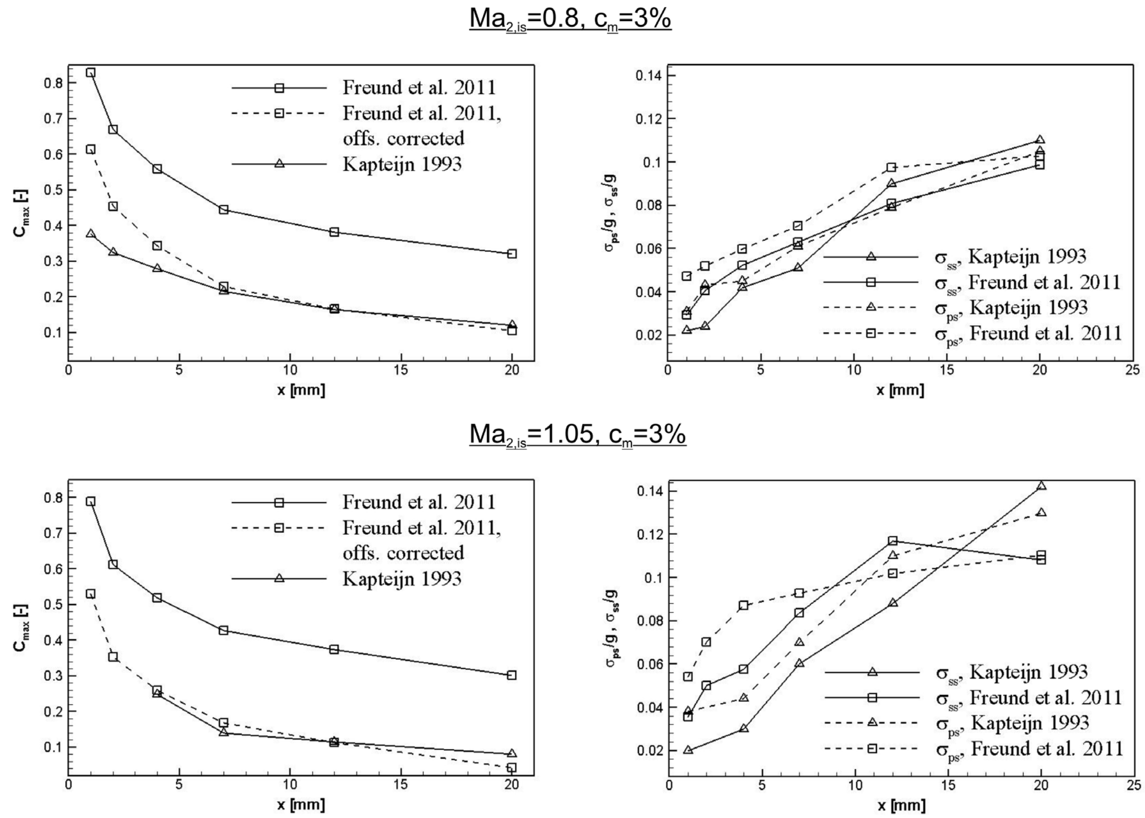


**FIGURE 11**. Comparison to $CO_2$ measurements: maximum concentration (left), cooling air flow width (right)

effect.

Figure 12 presents the standard deviation of the QLS measurements at different coolant mass flow ratios for $Ma_{2,is} = 1.05$. The comparable low standard deviation at $c_m = 1\%$ increases for the investigated wake (upper profile) by increasing the coolant mass flow ratio to 2%. In case of a coolant mass flow ratio of 3% the standard deviations increases again.

## CONCLUSIONS

Two different optical measurements techniques are carried out to investigate the influence of the cooling air ejection on the main flow on the one hand and to analyze the development of the cooling air concentration in exit flow direction on the other hand. The advantage of the same components used in the two measurements techniques leads to one identical experimental setup. The investigations on the effect of cooling air ejection by PIV clearly shows the reduction of the trailing edge shock by increasing the coolant mass flow ratio $c_m$. Furthermore, the shock front is moved upstream due to the movement of the point of flow deflection. Both effects can be observed in the numerical results as well.

Analyzing the cooling air concentration development by the QLS measurement technique leads to the conclusion that the maximum concentration is decreasing and the width of the wake is expanding with rising distance to the trailing edge. Furthermore, the cause of the mixing process is identified due to the velocity gradient in the shearing layer between the main flow and the cooling air flow. To validate the QLS measurement results, a comparison to $CO_2$ measurement results is performed. Apart from an offset in the development of the maximum concentration caused by the referencing step in the QLS measurement correction procedure the results are in good agreement. The benefit in measurement time in contrast to conventional probe measurements and its non intrusiveness provide the QLS technique as a very attractive alternative.

Besides the general improvement of the QLS measurement technique the independence of the PIV-QLS test procedure from calibration by an additional standard concentration measurement method should be an important issue for future research. One possibility could be the combination of the velocity field and the measured QLS concentration distribution. Under consideration of an integral constraint a correlation between the local values of

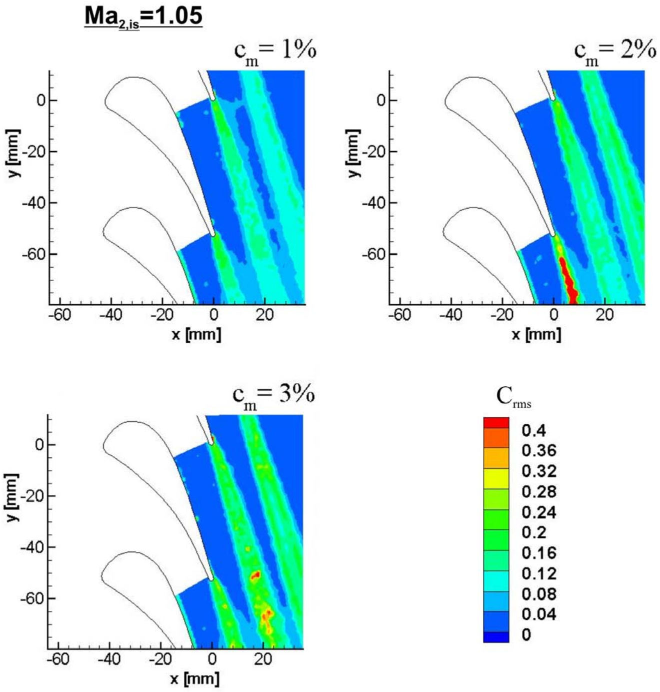


**FIGURE 12**. QLS standard deviation

the concentration and the velocity has to be found. The calculation of the blow-out velocity of the cooling air by the pressure in the cooling air supply line and the blow-out geometry could possibly deliver the missing referencing value.

## REFERENCES


[1] Wilcock, R., Young, J., and Horlock, J., 2005. "The effect of turbine blade cooling on the cycle efficiency of gas turbine power cycles". *Journal of Engineering for Gas Turbines and Power,* ***127***, p. 109.

[2] Bunker, R., 2007. "Gas turbine heat transfer: Ten remaining hot gas path challenges". *Journal of Turbomachinery,* ***129***, p. 193.

[3] Martini, P., Schulz, A., Whitney, C., and Lutum, E., 2003. "Experimental and numerical investigation of trailing edge film cooling downstream of a slot with internal rib arrays". *Proceedings of the Institution of Mechanical Engineers, Part A: Journal of Power and Energy,* ***217***, pp. 393–401.

[4] Chen, Y., Matalanis, C., and Eaton, J., 2008. "High resolution piv measurements around a model turbine blade trailing edge film-cooling breakout". *Experiments in Fluids,* ***44***, pp. 199–209.

[5] Sieverding, C., 1983. "The influence of trailing edge ejection on the base pressure in transonic turbine cascades". *ASME Journal of Engineering for Power,* ***105***, pp. 215–222.

[6] Kapteijn, C., Amecke, J., and Michelassi, V., 1996. "Aerodynamic performance of a transonic turbine guide vane with trailing edge coolant ejection: Part I- experimental approach". *ASME Journal of Turbomachinery,* ***118***, pp. 519–528.

[7] Raffel, M., and Kost, F., 1998. "Investigation of aerodynamic effects of coolant ejection at the trailing edge of a turbine blade model by PIV and pressure measurements". *Experiments in Fluid,* ***24***, pp. 447–461.

[8] Voigt, P., and Schodl, R., 1998. "Using the laser light sheet technique in combustion research". In AGARD conference proceedings, AGARD, pp. 48–1.

[9] Voigt, P., 1998. "Non-linear effects in planar scattering techniques: proofs of existence, simulations and numerical corrections of extinction and multiple scattering". In Proc. 9th Int. Symp. on Applications of Laser Techniques to Fluid Mechanics (Lisbon), pp. 26–2.

[10] Hassa, C., Migueis, C., Voigt, P., and Box, P., 1998. "Design principles for the quench zone of rich-quench-lean combustors". In 1st AVT-PPS Symposium on Design Principles and Methods for Aircraft Gas Turbine Engines, Toulouse, Vol. 11, p. 15.

[11] Jakirlić, S., Kniesner, B., Kadavelil, G., Gnirß, M., and Tropea, C., 2009. "Experimental and Computational Investigations of Flow and Mixing in a Single-Annular Combustor Configuration". *Flow, turbulence and combustion,* ***83***(3), pp. 425–448.

[12] Gnirß, M., and Tropea, C., 2008. "Simultaneous PIV and concentration measurements in a gas-turbine combustor model". *Experiments in fluids,* ***45***(4), pp. 643–656.

[13] Langowsky, C., 1997. Wechselwirkung von Sekundärströmung und Kühlluft in filmgekühlten Turbinenstatoren. DLR-Forschungsbericht 1997-50, German Aerospace Center.

[14] Dunker, R., 1995. *Advances in engine technology*. John Wiley and Sons.

[15] Nobach, H., Damaschke, N., and Tropea, C., 2005. "High-precision sub-pixel interpolation in particle image velocimetry image processing". *Experiments in Fluids 39,* ***2***, pp. 299–304.

[16] Raffel, M., Willert, C., and Wereley, S., 2007. *Particle image velocimetry: a practical guide*. Springer Verlag.

[17] Gnirß, M., and Tropea, C., 2008. "Simultaneous PIV and concentration measurements in a gas-turbine combustor model". *Experiments in fluids,* ***45***, pp. 643–656.

[18] Findeisen, J., Gnirß, M., Damaschke, N., Schiffer, H., and Tropea, C., 2005. "2D–Concentration Measurements Based on Mie Scattering using a Commercial PIV system". In 6th International Symposium on Particle Image Velocimetry, Pasadena, California, USA.

[19] Nürnberger, D., Eulitz, F., Schmitt, S., and Zachcial, A., 2001. "Recent progress in the numerical simulation of unsteady viscous multistage turbomachinery flow".

[20] Engel, K., Eulitz, F., Faden, M., and Pokorny, S., 1994. "Numerical investigation of the shock induced interaction in a transonic compressor stage". *American Society of Mechanical Engineers. Aerospace Division. Publication AD.,* ***40***, pp. 105–112.

[21] Engel, K., Nürnberger, D., Schmitt, S., and Yamamoto, K., 1998. "On recent advances of a time-accurate parallel navier-stokes solver for unsteady turbomachinery flow".

[22] Wilcox, D., of Aeronautics, A. I., and Astronautics, 1998. "Turbulence modeling for cfd".

[23] Durbin, P., Reif, B., and Reif, B., 2001. *Statistical theory and modeling for turbulent flows*. Wiley Online Library.

[24] Menter, F., Langtry, R., Likki, S., Suzen, Y., Huang, P., and Völker, S., 2006. "A correlation-based transition model using local variables-part I: model formulation". *Journal of Turbomachinery, **128***, p. 413.